Different manifestations of accretion onto compact objects

Altamirano, D.

5 The Island state of the Atoll Source 4U 1820–30

Diego Altamirano, M. van der Klis, M. Méndez, S. Migliari, P.G. Jonker, A. Tiengo and W. Zhang

Astrophysical Journal, 2005, 633, 358

Abstract

We study the rapid X-ray time variability in all public data available from the *Rossi X-ray Timing Explorer's* Proportional Counter Array on the atoll source 4U 1820–30 in the low-luminosity island state. A total of ~ 46 ks of data were used. We compare the frequencies of the variability components of 4U 1820–30 with those in other atolls sources. These frequencies were previously found to follow a universal scheme of correlations. We find that 4U 1820–30 shows correlations that are shifted by factors of 1.13 ± 0.01 and 1.21 ± 0.02 with respect to those in other atoll sources. These shifts are similar to, but smaller than the shift factor ~ 1.45 previously reported for some accreting millisecond pulsars. Therefore, 4U 1820–30 is the first atoll source which shows no significant pulsations but has a significant shift in the frequency correlations compared with other 3 non-pulsating atoll sources.

5.1 Introduction

Accretion in neutron star low-mass X-ray binaries (LMXBs) can be studied through the spectral and timing properties of the associated X-ray emission. The Fourier power spectra of the X-ray flux of these systems, exhibit quasi-periodic oscillations (QPOs) as well as noise components between $\sim 1 \times 10^{-3}$ Hz and $\sim$ 1350 Hz. Most of these variability components are thought to be associated with processes in the accretion disk (for reviews and references see van der Klis 2000, 2004) but some of them may arise on the surface of the neutron star (see e.g. Revnivtsev et al. 2001; Strohmayer & Bildsten 2003). The timing properties at low frequencies ($\nu < 100$ Hz) as well as the spectral properties are the basis of the classification of these systems as either Z or atoll sources (Hasinger & van der Klis 1989). In recent literature, each variability component is designated L_i – L for 'Lorentzian', Belloni et al. (2002b) – where the index i indicates the component; the component's characteristic frequency is designated ν_i. For example, L_b is an often flat-topped broad band noise component at a low frequency ν_b, and L_u the upper kilohertz QPO with frequency ν_u (see van Straaten et al. 2003, for complete terminology).

The kilohertz QPOs are seen between a few hundred and $\sim$ 1350 Hz and when two of them are seen at the same time (twin kHz QPOs), the difference between their frequencies is constrained between $\sim$ 185 Hz and $\sim$ 400 Hz. In the 0.01-100 Hz range two to five band-limited noise, peaked-noise and QPO components are observed whose frequencies all correlate with one another and with that of the kilohertz QPOs (see van Straaten et al. 2005, and references within). An example is the WK correlation (after Wijnands et al. 1999), between the hump frequency ν_h and the break frequency ν_b. This relation may be fundamental in the understanding of the processes of accretion in LMXBs because, in atoll sources and black holes ν_b and ν_h correlate over 3 orders of magnitude (the Z sources have slightly higher ν_h). The existence of such correlations suggests that similar physical phenomena may be responsible for some of the QPOs and noise components found over wide ranges of frequency and coherence in Z, atoll and black hole sources.

van Straaten et al. (2005) found that the frequencies of the noise and QPO components of the accreting millisecond pulsar SAX J1808.4–3658 also correlate with ν_u, but, in a different way than those of the other atoll sources.

They interpreted the difference between the pulsar and the atoll sources as due to a shift in frequency of the upper kilohertz QPO and suggested that physical differences between these sources are most likely to affect the high frequency components. In SAX J1808.4-3658, the factors by which ν_u had to be multiplied to make the correlations coincide with those of the ordinary atoll

sources were 1.420 ± 0.013 for ν_b, and 1.481 ± 0.013 for ν_h.

4U 1820–30 is a low-mass X-ray binary with an orbital period of only 11.4 minutes (Stella et al. 1987) and an X-ray burst source (Grindlay et al. 1976). It is located in the globular cluster NGC 6624 at a distance 7.6 ± 0.4 kpc (Kuulkers et al. 2003a). Radio emission has also been detected from the source (Geldzahler 1983; Migliari et al. 2004). 4U 1820–30 undergoes a regular ~ 176 day accretion cycle (Priedhorsky & Terrell 1984a), switching between high and low states differing by a factor $\sim$3 in luminosity (Strohmayer & Brown 2002). The ultra-compact nature of the system requires that the secondary is a low-mass helium dwarf (see e.g. Rappaport et al. 1987) so that the accreted material likely has a very low hydrogen abundance. Hasinger & van der Klis (1989) defined 4U 1820–30 as an atoll source and eight years later Smale et al. (1997) reported the discovery of kHz quasi-periodic oscillations. Zhang et al. (1998c) reported the result from a long-term monitoring data set obtained with the Rossi X-ray Timing Explorer. They observed kHz QPOs in both the lower banana and the island state (see van der Klis 2004, for nomenclature). They showed that the frequency of the kilohertz QPOs is correlated with the PCA count rate below a critical value (~ 2500 counts s^{-1} per 5 PCUs). Above this, the QPO frequencies remained constant while the count rate increased between ~ 2500 and ~ 3200 counts s^{-1} per 5 PCUs. Saturation of QPO frequency at high mass accretion rates is an expected signature of the marginally stable orbit (Miller et al. 1998; Kaaret et al. 1999); however, this is the only source reported to have shown this behavior, and to what extent count rate is a good indicator of accretion rate remains to be seen (see, e.g. the discussion of the issue in van der Klis 2001). Later, similar analysis were carried out, using instead of the count rate, (i) the energy flux, (ii) the X-ray spectral shape (Kaaret et al. 1999) and (iii) the parameter S_a (Bloser et al. 2000) which parameterizes atoll source location in the track of the color-color diagram. The same behavior as that observed by Zhang et al. (1998c) as a function of count rate was found, when the QPO frequency was plotted as a function of either of these three parameters. The saturation of QPO frequency was interpreted as strong additional evidence for the detection of the marginally stable orbit in the accretion disk of 4U 1820–30. However, since then Méndez (2002) has argued that the evidence of the saturation is not so compelling, especially when some instrumental corrections are taken into account. A general tendency for QPO frequency to saturate toward higher luminosity may be a feature of the same phenomenon that produces the parallel tracks in frequency-luminosity diagrams (van der Klis 2001).

In this paper, we report on the eight observations that are currently available of 4U 1820–30 in the island state. All previous works mentioned above

included only one observation (20075-01-05-00) of the source in the island state, so the current analysis better allows us to constrain the power spectral components in the island state of 4U 1820–30 more accurately. We study the correlations between the characteristic frequencies of the various timing features, and compare these with those of four well-studied atoll sources, three low-luminosity bursters, one Z-source and one accreting millisecond pulsar. We show that the correlations between frequencies in 4U 1820–30 are shifted as found for SAX J1808.4–3658, but with a lower shift factor. We finally discuss whether the interpretation of a multiplicative shift of frequencies is the right explanation for the differences in frequency behavior between the millisecond accreting pulsar SAX J1808.4–3658 and the ordinary atoll sources.

5.2 Observations and data analysis

We used all public data available from the Rossi X-ray Timing Explorer's (RXTE) Proportional Counter Array (PCA; for instrument information see Zhang et al. 1993). There were 158 pointed observations in 9 programs (10074, 10075, 10076, 20075, 30053, 30057, 40017, 40019, 60030, 70030 and 70031). In our analysis, we use the 16-s time-resolution Standard 2 mode data to calculate X-ray colors. For each of the five PCA detectors (PCUs) we calculate a hard and a soft color defined as the count rate in the 9.7–16.0 keV band divided by the rate in the 6.0–9.7 keV band and the 3.5–6.0 keV rate divided by the 2.0–3.5 keV rate, respectively. For each detector we also calculate the intensity, defined as the count rate in the energy band 2.0–16 keV. To obtain the count rates in these exact energy ranges, we interpolate linearly between count rates in the PCU channels.We then subtract the background contribution in each band using the standard bright source background model for the PCA, version 2.1e [1]. No deadtime corrections were made as the effect of deadtime can be neglected for our purposes ($< 0.001\%$). We calculate the colors and intensity for each time interval of 16s. In order to correct for the gain changes as well as the differences in effective area between the PCUs themselves, we used the method introduced by Kuulkers et al. (1994): for each PCU we calculate, in the same manner as for 4U 1820–30, the colors of the Crab which can be supposed to be constant. We then average the 16s Crab colors and intensity for each PCU for each day. For each PCU we divide the 16s color and intensity values obtained for 4U 1820–30 by the corresponding Crab values that are closest in time but in the same RXTE gain epoch. The RXTE gain epoch changes with each new high voltage setting of the PCUs (Jahoda et al. 1996). After the Crab normalization is done, we average the colors and intensity over all

[1] PCA Digest at http://heasarc.gsfc.nasa.gov/ for details of the model

PCUs. Finally, we average the 16s colors per observation. Figure 5.1 shows the color-color diagram of the 158 different observations that we used for this analysis, and Figure 5.2 the corresponding hardness-intensity diagrams (soft and hard color vs. intensity).

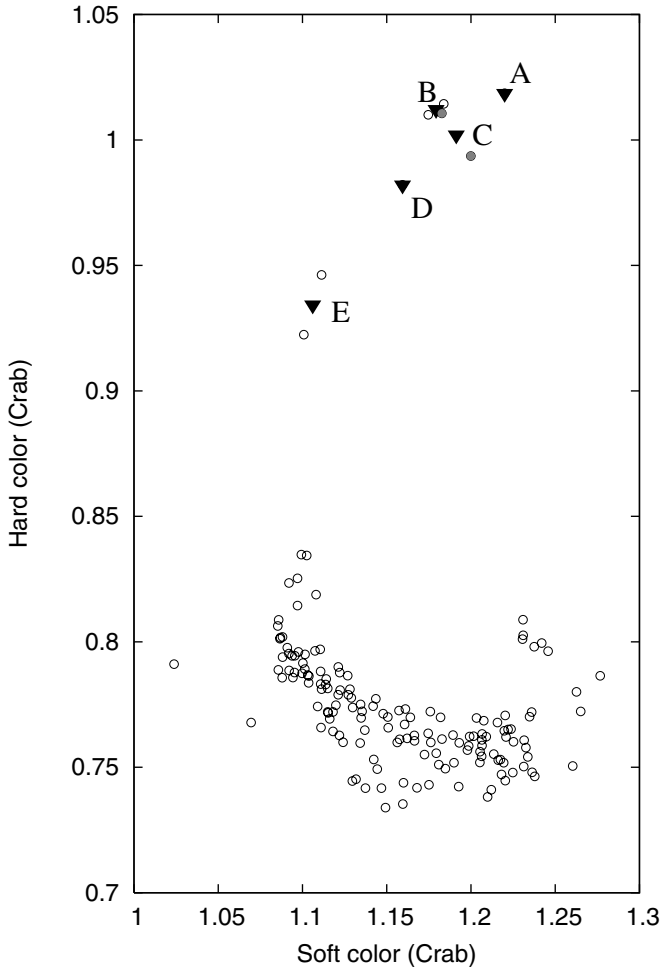

Figure 5.1: 4U 1820–30's hard color vs. soft color normalized to Crab colors as explained in Section 5.1. Each circle represents one of the 158 observations mentioned in Section 5.2. The triangles represent the average power spectra A to E. They correspond to one or two observations and are labeled in order of decreasing average hard color. For clarity, the two grey-filled circles represent the two observations averaged to get power spectrum C. The error bars are of the order of the size of the symbols.

We find 8 observations which are located in the island region of the color-

color diagram (hard colors greater than 0.9). These observations are the subject of this paper (see Table 5.1).

Hard Color	Observation ID	Label	Date of Observation	Duration (ks)	Number of PCUs on	Average (c/s/PCU)
1.018	40017-01-24-00	A	Jun-04-2003	~ 8.2	3	~ 268
1.010	70030-03-04-00	B	Jun-11-2003	~ 3.2	4	~ 281
1.014	70030-03-05-00	B	Jun-14-2003	~ 6.5	4	~ 308
0.993	70030-03-04-01	C	Jun-12-2003	~ 6.5	3	~ 283
1.010	70030-03-05-01	C	Jun-15-2003	~ 6.6	3	~ 358
0.982	70031-05-01-00	D	Jun-14-2002	~ 3.1	5	~ 297
0.922	20075-01-05-00	E	May-02-1997	~ 8.5	5	~ 354
0.946	70030-03-05-02	E	Jun-16-2003	~ 3.2	2	~ 421

Table 5.1: The eight observations used for the timing analysis. The statistical errors in hard color are $\lesssim 0.001$.

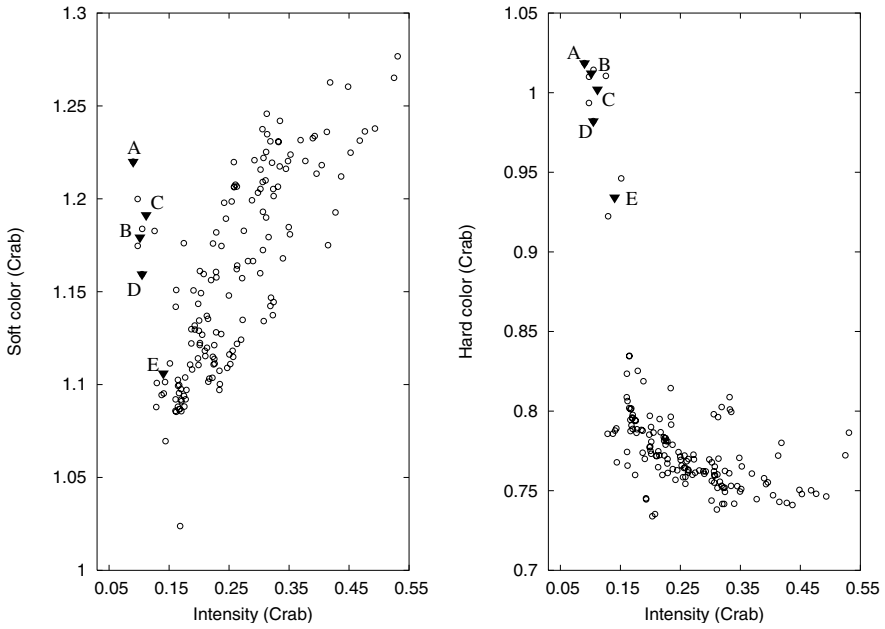

Figure 5.2: Soft color vs. intensity (left) and hard color vs. intensity (right) in Crab units as explained in Section 5.1. Symbols as in Figure 5.1. The error bars are of the order of the size of the symbols.

For the Fourier timing analysis of these 8 observations we used an 125μs time resolution Event mode (E_125us_64M_0_1s). Leahy-normalized power spectra were constructed using data segments of 128 seconds and 1/8192s time bins such that the lowest available frequency is $1/128 \approx 8 \times 10^{-3}$ Hz

and the Nyquist frequency 4096 Hz. Detector drop-outs were removed but no background or deadtime corrections were performed prior to the calculation of the power spectra. We first averaged the power spectra per observation. We inspected the shape of the average power spectra at high frequency ($>$ 2000 Hz) for unusual features in addition to the usual Poisson noise. None were found. We then subtracted a Poisson noise spectrum estimated from the power between 3000 and 4000 Hz, where neither intrinsic noise nor QPOs are known to be present, using the method developed by Klein-Wolt (2004) based on the analytical function of Zhang et al. (1995). The resulting power spectra were then converted to squared fractional rms (van der Klis 1995a). In this normalization the square root of the integrated power density is a direct measurement of the variance caused by the intrinsic variability in the source count rate. In three cases it was possible to add two observations together to improve statistics. This was done only for those observations which had similar colors and power spectra consistent with being the same within errors. The resulting power spectra are labeled from A to E (Figure 5.3) in order of decreasing hard color. Table 5.1 shows which observations were used to create each of the averaged power spectra.

To fit the power spectra, we used a multi-Lorentzian function: the sum of several Lorentzian components plus, if necessary, a power law to fit the very low frequency noise (VLFN). Each of these components, is usually described with an L_i (for 'Lorentzian') and its frequency, with ν_i, where i determines the type of component. For example, L_u identifies the upper kHz QPO and ν_u its frequency. By analogy, other components go by names such as L_ℓ (lower kHz), L_{hHz} (hectohertz), L_h (hump), L_b (break frequency), and their frequencies as ν_ℓ, ν_{hHz}, ν_h and ν_b, respectively. Using this multi-Lorentzian function makes it straightforward to directly compare the different components in 4U 1820–30 to those in previous works which used the same fit function (e.g., Belloni et al. 2002b; van Straaten et al. 2003, 2005, and references therein).

In the fits we only include those Lorentzians with a significance larger than 3σ based on the error in the power integrated from 0 to ∞. We give the results of the fits in terms of ν_{max} and Q, of which ν_{max} was introduced by Belloni et al. (2002b) as $\nu_{max} = \sqrt{\nu_0^2 + (\frac{FWHM}{2})^2} = \nu_0\sqrt{1 + \frac{1}{4Q^2}}$. For Q we use the standard definition $Q = \frac{\nu_0}{FWHM}$. FWHM is the full width at half maximum of the Lorentzian.

5.3 Results

Figures 5.1 and 5.2 show that in order A to E, the spectrum becomes softer, i.e. both hard and soft color decrease, while the spectrum is harder than in

the banana branch and the intensity is approximately constant (see Figure 5.2). This is the expected behavior for an atoll source which is moving from the island to the lower left banana state in the color color diagram (van der Klis 2004).

In Figure 5.3, we show the average power spectra with their fits. Four to five Lorentzian components were needed for a good fit of power spectra A–D. Power spectrum E, whose colors are closest to the upper banana state, could be fitted with either six or seven Lorentzians. Both fits share six components whose frequencies are the same within errors; in the case of 7 Lorentzians, an extra component is present at $\nu_3 = 407.9 \pm 30.5$. This component is significant only at $\sim 2\sigma$ (single trial) level, and represents an $\sim 1.3\sigma$ improvement of the χ^2 of the fit according to an F-test. However, if this component, which is consistent with being the lower kilohertz QPO peak, is not included in the model, the fit becomes unstable unless the quality factor Q_{hHz} is fixed.

Table 5.2 gives the results of the fits to the power spectra and in Figure 5.4, we show the correlations of the characteristic frequencies ν_{max} of the power spectral components with the frequency of the upper kilohertz QPO ν_u. For power spectrum E, we always show the results for 7 Lorentzians.

As expected for the island state of an atoll source, ν_u is lower than ~ 700 Hz (see e.g. van Straaten et al. 2003, 2005; van der Klis 2004) and increases monotonically from A to E with decreasing hard color. L_{hHz} is at similar frequencies as in the other atoll sources, between ~ 100 and ~ 200 Hz.

For L_b and L_h, a shift appears to exist between the correlations of 4U 1820–30 and those of the other atoll sources studied by van Straaten et al. (2005). To further investigate this, in Figures 5.5 and 5.6 we plot ν_b and ν_h respectively, versus ν_u. We use all the data used by van Straaten et al. (2005) for the atoll sources and the low luminosity bursters; however, of the millisecond pulsars, we only use data of SAX J1808.4–3658, which, in contrast to the others, has data points in the same frequency region as 4U 1820–30. As can be seen in Figures 5.5 and 5.6, our points for 4U 1820–30 are right in the important transition region around $\nu_u \sim 600$ Hz. On one hand for L_b (Figure 5.5), our points seem to link the SAX J1808.4–3658 data with those for the atoll sources with $\nu_u \gtrsim 600$ Hz. However, neither the frequency range covered by 4U 1820–30 nor SAX J1808.4–3658 is sufficient to draw the conclusion that the two different correlations below $\nu_u \sim 600$ Hz become the same correlation above $\nu_u \sim 600$ Hz, as the figure seems to suggest. On the other hand, as shown in Figure 5.6, in 4U 1820–30 the L_h points seem to lie between those of the atoll sources and those of SAX J1808.4–3658.

To determine the shift factors between the frequency correlations of 4U 1820–30 and those of the other atoll sources, and to be able to compare them

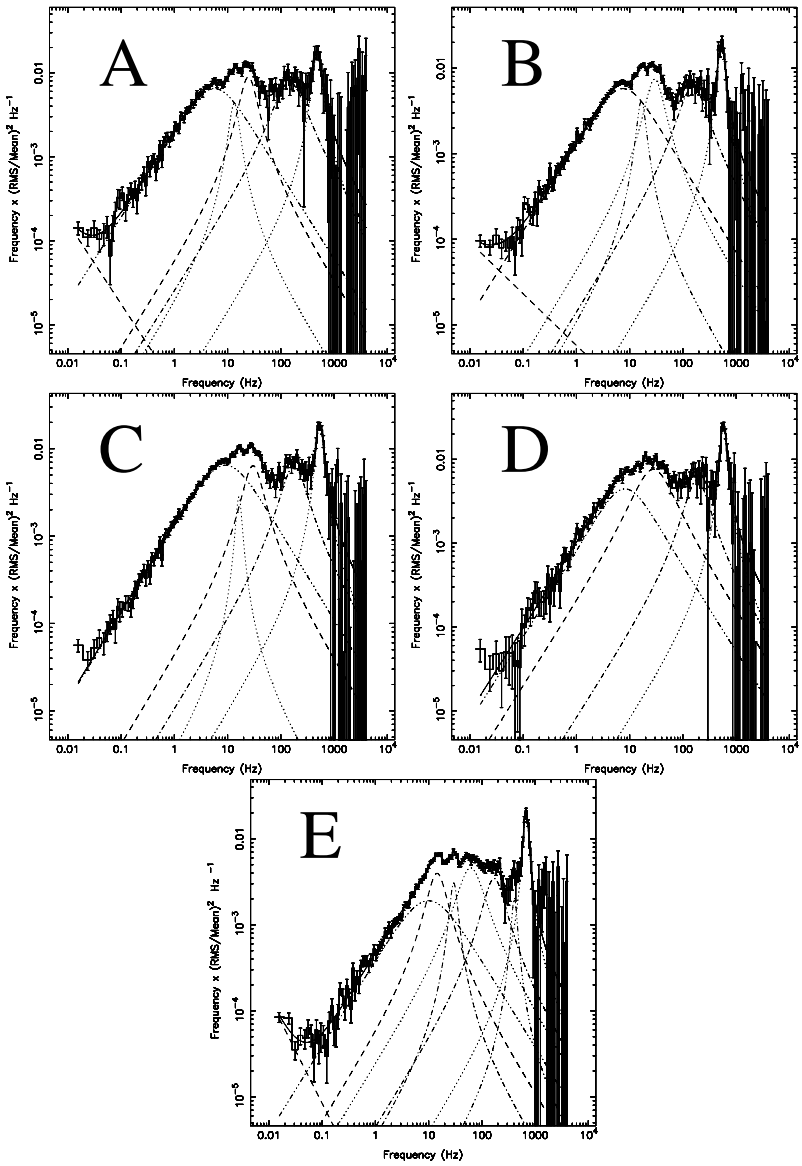

Figure 5.3: Power spectra and fit functions in the power spectral density times frequency representation for 4U 1820–30. Each plot corresponds to a different position in the color-color and color intensity diagrams (see Figures 5.1 and 5.2). The different lines mark the individual Lorentzian components of the fit. For a detailed identification, see Table 5.2, Figure 5.4 and Section 5.3.

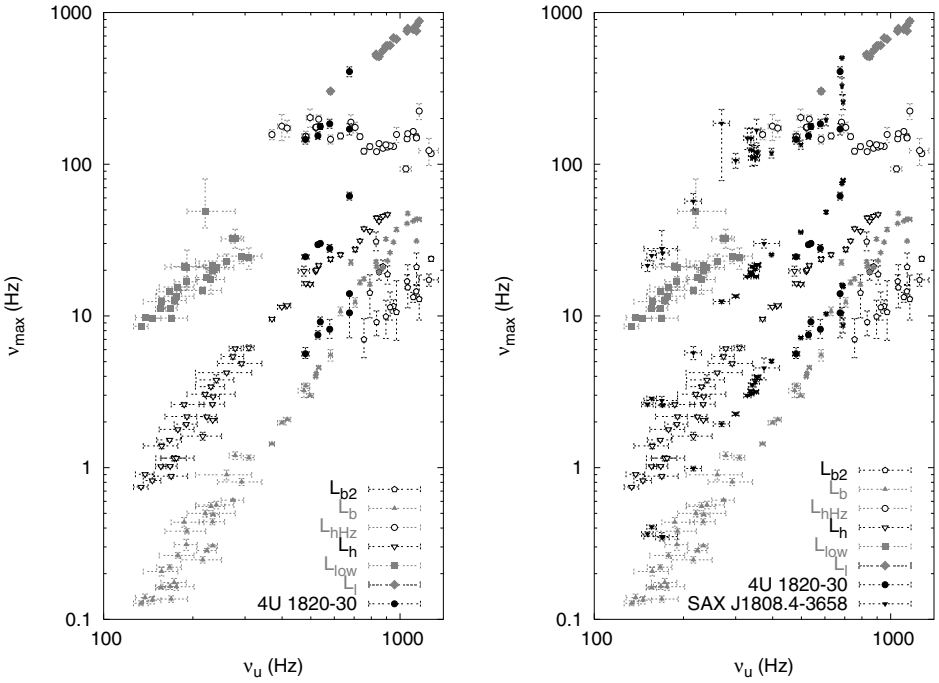

Figure 5.4: Correlations between the characteristic frequencies ν_{max} of the various power spectral components and ν_u. For clarity, on the *left* we plot the different components of the atoll sources 4U 0614+09, 4U 1608–52, 4U 1728–34 and Aql X-1 and the low luminosity bursters 1E 1724–3045, GS 1826–24 and SLX 1735–269 (van Straaten et al. 2005), where the black bullets mark the results for the island state features of 4U 1820–30. On the *right*, we show the same plot as on the left, but we include the results for the millisecond accreting pulsar SAX J1808.4–3658 (black triangles).

with the shift factors found for SAX J1808.4–3658, we followed the same procedure as used by van Straaten et al. (2005): we considered the ν_b vs. ν_u and ν_h vs. ν_u relations for which $\nu_u < 600$ Hz, as the behavior of the low-frequency components above 600 Hz is complex. In practice, this means that we exclude power spectrum E. Note that in our analysis we included the data point for SAX J1808.4–3658 at $\nu_u = 497.6 \pm 6.9$ Hz that, when shifted, ends up above 600 Hz, and which was excluded by van Straaten et al. (2005).

For each relation, we fit a power law to the 4U 1820–30 frequencies together with those of the atoll sources using the FITEXY routine by Brian P. Flannery & Vetterling (1989), which performs a straight line fit to data with errors in both coordinates. We took the logarithm of the frequencies so that fitting a power law becomes equivalent to fitting a straight line. Before fitting, we multiplied the 4U 1820–30 ν_u values with a shift factor that ran between 0.1 and 3 with steps of 0.001. The fit with the minimal χ^2 then gave the best shift factor. The errors in the shift factor use $\Delta\chi^2 = 1$, corresponding to a 68% confidence level.

The best shift factors in ν_u for 4U 1820–30 are 1.21 ± 0.02 ($\chi^2/dof = 19.4/18$) and 1.13 ± 0.01 ($\chi^2/dof = 45.3/18$) for ν_b and ν_h respectively.

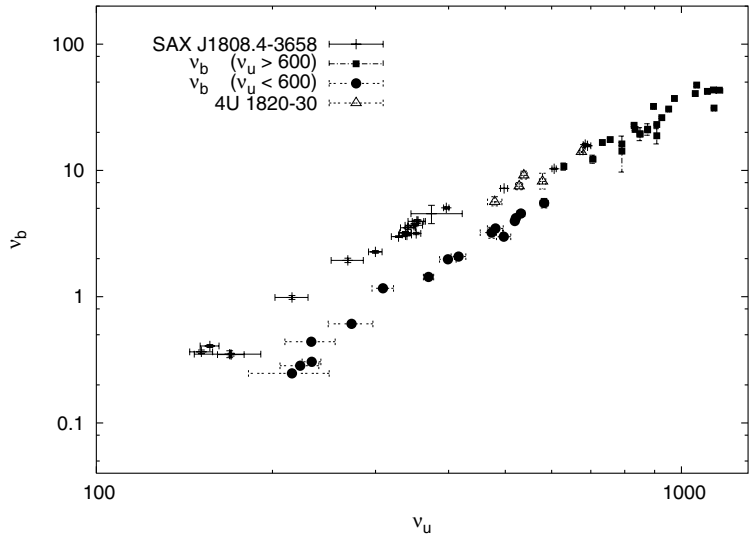

Figure 5.5: Correlation between the characteristic frequencies ν_b and ν_u. The black circles and the black squares mark the atoll sources 4U 0614+09, 4U 1608–52, 4U 1728–34 and Aql X-1 and the low luminosity bursters 1E 1724–3045, GS 1826–24 and SLX 1735–269 (van Straaten et al. 2005) for $\nu_u < 600$ Hz and $\nu_u > 600$ Hz, respectively. The open triangles mark the results for 4U 1820–30 and the crosses represent the results from van Straaten et al. (2005) for SAX J1808.4–3658.

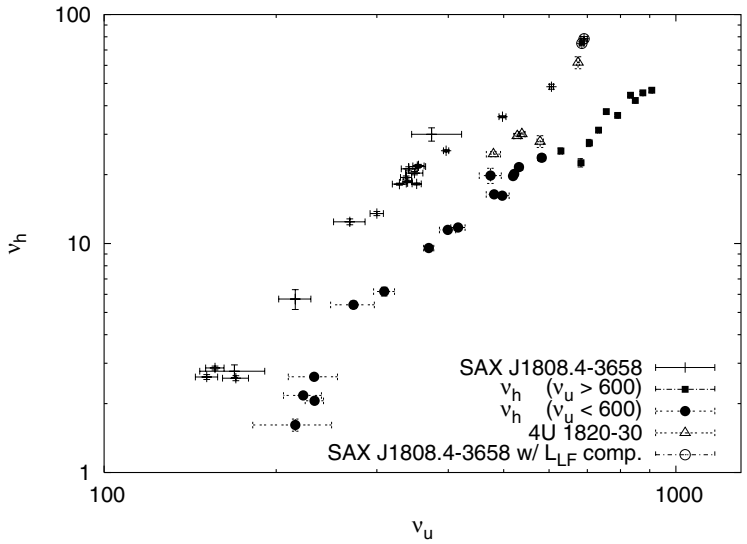

Figure 5.6: Correlation between the characteristic frequencies ν_h and ν_u. Symbols as in Figure 5.5. The two open circles represent the results for SAX J1808.4-3658 in which a L_{LF} component was also found (see van Straaten et al. 2005).

If we repeat the procedure described above, but this time instead of multiplying ν_u, we multiply ν_b and ν_h by a variable factor (vertical frequency shifts in Figure 5.4) , the best shift factor in ν_b is 0.55 ± 0.03 ($\chi^2/dof = 19.4/18$) and in ν_h is 0.73 ± 0.02 ($\chi^2/dof = 45.3/18$). Clearly, the high χ^2 when calculating the best fit for ν_h indicates that the dispersion of the data around the power law is larger than expected from counting statistics.

In Figure 5.7 we plot the characteristic frequency ν_h versus ν_b. As van Straaten et al. (2005) showed, the millisecond pulsar SAX J1808.4–3658 follows approximately the same correlation as the atoll sources and low luminosity bursters at frequencies $\nu_b \lesssim 3$ Hz. For $3 \lesssim \nu_b \lesssim 5$ Hz, the atoll sources slightly deviate, as ν_b increases, toward lower ν_h. For $\nu_b \gtrsim 5$, van Straaten et al. (2005) observed a non-continuous bifurcation where ν_b of the atoll sources jumps to higher frequencies while SAX J1808.4–3658 smoothly extends the correlation observed for $\nu_b \lesssim 3$ Hz. Our new data for 4U 1820–30, which are all at $\nu_b > 5$ Hz, seem to be in between these two correlations, apparently following the behavior of the atoll sources for $3 \lesssim \nu_b \lesssim 5$ Hz. However, the point for 4U 1820–30 at higher ν_b (and higher ν_h), falls in the correlation of SAX J1808.4–3658.

In Figure 5.7 we also show the frequency of the Horizontal Branch Oscillation (HBO) and its subharmonic versus that of the Low Frequency Noise (LFN) for the Z-source GX 5–1. The data of GX 5–1 was taken from van

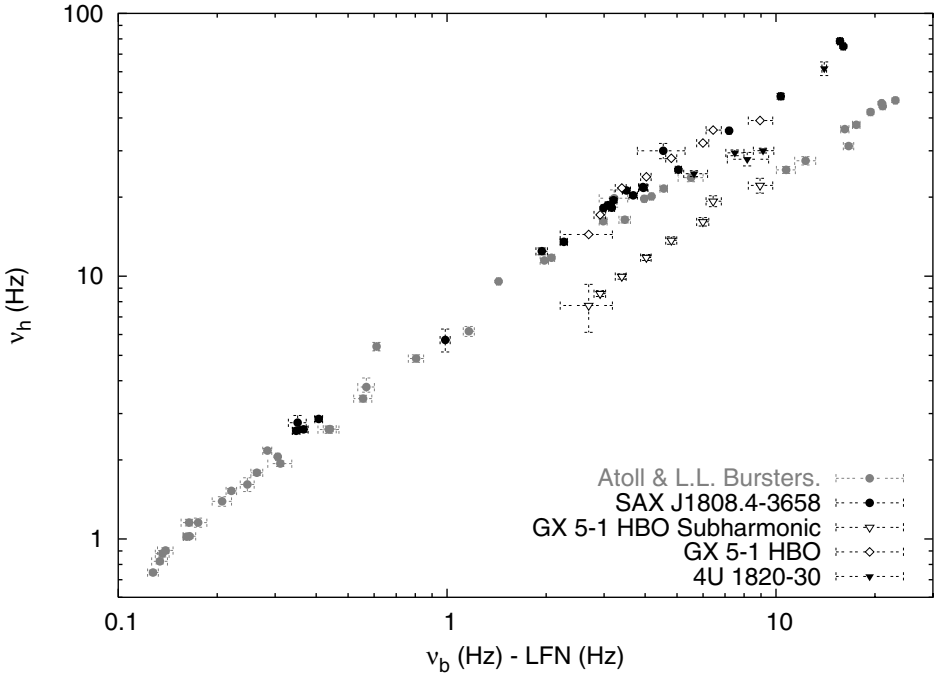

Figure 5.7: The characteristic frequency ν_h plotted versus ν_b. The grey circles mark the atoll sources 4U 0614+09, 4U 1608–52, 4U 1728–34, Aql X-1 and the low luminosity bursters 1E 1724–3045, GS 1826–24 and SLX 1735–269. The black circles mark the accreting millisecond pulsar SAX J1808.4–3658 (van Straaten et al. 2005). The filled triangles mark the results for 4U 1820–30. We also include the HBO and HBO subharmonic characteristic frequencies of the Z-source GX 5–1 (open diamonds and open triangles, respectively), plotted versus that of the low frequency noise (LFN) (van Straaten et al. 2003).

Straaten et al. (2003) (but see Jonker et al. 2002a, for original data). The HBO component of GX 5–1 follows the same correlation as SAX J1808.4–3658 but, as already noted by Wijnands et al. (1999), the HBO of Z-sources is slightly higher in this diagram than the L_h and L_{LF} components of atoll sources. The HBO subharmonic extends the correlation that is found for atoll sources and low luminosity bursters for $\nu_b \gtrsim 5$ Hz to lower frequencies, suggesting that the apparent bifurcation mentioned before could be associated with harmonic mode switching.

In Figure 5.8 we plot the characteristic frequency of the narrow low-frequency QPOs ($Q \gtrsim 2.5$), which have characteristic frequency ν_{max} between ν_b and ν_h, versus ν_h. Such narrow QPOs were previously reported in other sources (e.g. van Straaten et al. 2003, 2005, and references within) and we also detect them in 4U 1820–30. Following van Straaten et al. (2003), for clarity we have omitted these QPOs (L_{LF}) from Figure 5.4. In Figure 5.8, the data of 4U 1820–30 seem to follow the power law fitted to the ν_{LF} vs. ν_h relation of the low-luminosity bursters 1E 1724–3045, GS 1826–24 and the Black Hole Candidate (BHC) GX 339–4 by van Straaten et al. (2003, 2005); therefore we identify these QPOs as being the L_{LF} component.

5.4 Discussion

We have performed the first detailed study of the fast time variability in the island state of the atoll source 4U 1820–30. It has been reported before that the frequencies of the variability components of the atoll sources follow a universal scheme of correlations when plotted versus ν_u (van Straaten et al. 2003, and references within). In Figure 5.4 (left) we show that our data are in general agreement with this scheme. Van Straaten et al. (2005) showed that the accreting millisecond pulsar SAX J1808.4–3658 shows similar relations between its characteristic frequencies as the atoll sources do, but shifted (Figure 5.4 - right). This shift was interpreted to occur only between the characteristic frequencies of the low frequency components on one hand and ν_u (and ν_ℓ) on the other, where ν_u (and ν_ℓ) had to be multiplied by ~ 1.45 to make the correlations coincide. Figures 5.5 and 5.6 suggest that this could also be the case for 4U 1820–30. However, the shift factor for ν_u is 1.21 ± 0.02 and 1.13 ± 0.01 for L_b and L_h, respectively, giving an average of 1.17 ± 0.01 which is smaller than the values of 1.420 ± 0.013 and 1.481 ± 0.013, respectively, giving an average of 1.454 ± 0.009 (van Straaten et al. 2005). Similar shift factors as we find for 4U 1820–30 may in fact be present in other accreting millisecond pulsars and faint burst sources; for example in XTE J1751–305, van Straaten et al. (2005) found shift factors of 1.188 ± 0.045 and 1.112 ± 0.042

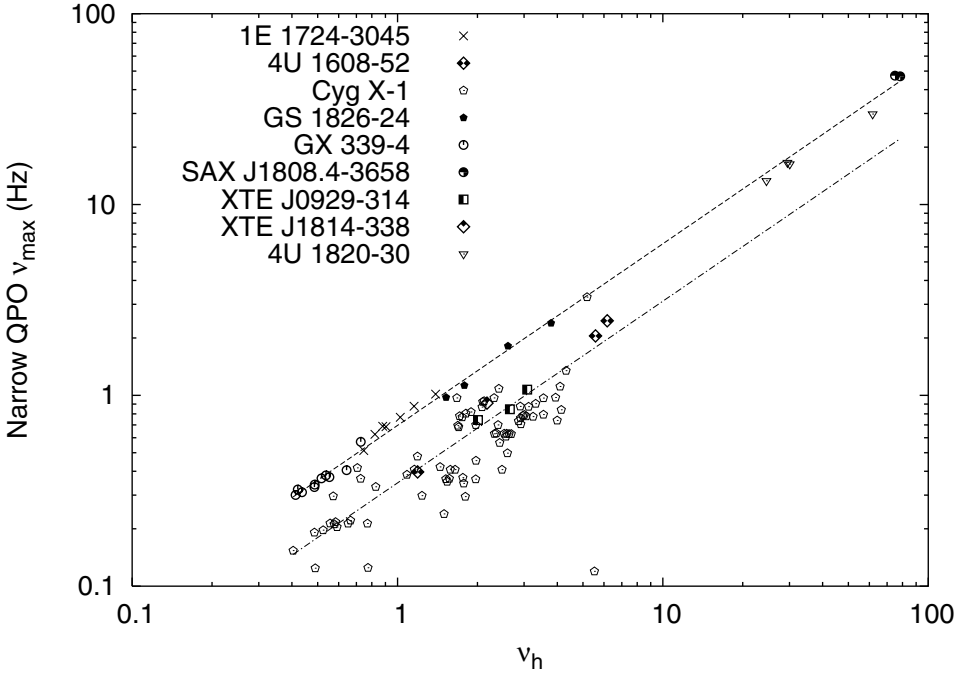

Figure 5.8: Characteristic frequencies ν_{LF} and $\nu_{LF/2}$ (see text) versus ν_h. The symbols are labeled in the plot, and represent the frequencies of the QPOs from the atoll source 4U 1608–52, the BHCs Cyg X–1 and GX 339–4, the low luminosity bursters 1E 1724–3045 and GS 1826–24 and the accreting millisecond pulsars XTE J0929–314, XTE J1814–338 and SAX J1808.4–3658 (van Straaten et al. 2003, 2005). The open triangles show the results for 4U 1820–30. The dashed line indicates a power law fit to the ν_{LF} vs. ν_h relation of the low-luminosity bursters 1E 1724–3045 and GS 1826–24, and the BHC GX 339–4. The dash-dotted line is a power law with a normalization half of that of the dashed line. The error bars are of the order of the size of the symbols.

for L_b and L_h, respectively. These results are consistent with our values, however, the results for XTE J1751–305 have larger errors. It is important to note that, XTE J1751–305 has a companion of 0.013-0.35 solar mass, suggesting a heated helium dwarf (Markwardt et al. 2002). Since 4U 1820–30 also has a low-mass helium dwarf, the similarity in frequency shifts might be related to the chemical composition of the material in the accreting disk. However, a simple "frequency shift–chemical composition" relation is not evident, since the composition of the companion stars of SAX J1808.4–3658, 4U 0614+09, 4U 1608–52 and 4U 1728–34 are uncertain. For instance, SAX J1808.4–3658 might have a brown dwarf, 4U 0614+09 might have an oxygen-carbon white dwarf and both 4U 1608–52 and 4U 1728–34 might have late type main sequence companions (but see Bildsten & Chakrabarty 2001; Nelemans et al. 2004; Wachter et al. 2002; Marti et al. 1998, respectively, for discussions).

van Straaten et al. (2005) suggested that the measured shift factors of $\sim 1.5 \equiv 3/2$ could be related with the parametric resonance models for kilohertz QPOs (e.g. Abramowicz et al. 2003), where the 2:3 frequency resonances between general relativistic orbital/epicyclic frequencies play a central role. The average shift factor for 4U 1820–30 is 1.17 ± 0.01, so we can reject the idea that 2:3 resonances are the (only) cause of the shifts.

We further attempted to test the hypothesis that a multiplicative shift of frequencies is the right interpretation of the difference in the frequency correlations between SAX J1808.4–3658 and the other atoll sources. If that hypothesis is correct, we should expect both correlations to have the same power law index within errors, and, the only significant difference between the correlations would arise from the normalization of each of the power laws. In order to quantify the differences, we performed two different fits where simultaneously a power law is fitted to the data of SAX J1808.4–3658, and another power law is fitted to the data of the atoll sources 4U 1608–52, 4U 0614+09 and 4U 1728–34. Then we compare the χ^2/dof of the fits. We only use data of the L_b components since L_h's behavior is more complex. If both power law indexes and normalizations are free parameters, the best fit gives a $\chi^2/dof = 60.2/30$. If we force both power laws to have the same index, but different normalizations, the best fit gives a $\chi^2/dof = 86.2/31$.

By comparing these results using an F-test, we find that the improvement of the fit when leaving all the parameters free as compared to forcing equal slopes is significant at the 3.4σ level. If the "shift" interpretation is correct, then the slopes of both correlations should be the same and then, we should not find a significant improvement of the fit. However, the fact that we are dealing with $\chi^2/dof \gtrsim 2$, reduces the statistical significance of our possible interpretations.

If we perform the same analysis between 4U 1820–30 and the atoll sources, we find χ^2_1/dof values of 19.4/16 and 19.6/17, i.e., no significant improvement of the fit. Therefore, in both cases the data are *not* inconsistent with the hypothesis that the differences between correlations are due to only a shift in ν_u (van Straaten et al. 2005).

As suggested by van Straaten et al. (2005), the simplest explanation for the shift between correlations, is that there is some physical difference between sources which affects ν_u. Up to now, such shifts had only been seen in accreting pulsars and only at high confidence in SAX J1808.4–3658, which led to the suggestion that the same source property that leads to strong pulsations also affects ν_u (van Straaten et al. 2005). 4U 1820–30 has no strong pulsations (Dib et al. 2005), invalidating any strict relation between these two characteristics. However, as the shifts in 4U 1820–30 are smaller than in SAX J1808.4-3658 and, as accidental circumstances such as an unfavorable viewing geometry could suppress the pulsations in 4U 1820–30, it is too early to reject this idea.

Acknowledgments: DA likes to thank M. Linares and R. Wijnands for helpful discussions. This work was supported by the "Nederlandse Onderzoekschool Voor Astronomie" (NOVA), i.e., the "Netherlands Research School for Astronomy", and it has made use of data obtained through the High Energy Astrophysics Science Archive Research Center Online Service, provided by the NASA/Goddard Space Flight Center.

Power spectrum A			
ν_{max} (Hz)	Q	rms (%)	comp.
479.73 ± 13.65	2.47 ± 0.52	9.90 ± 0.82	L_u
145.80 ± 11.15	0.58 ± 0.17	11.80 ± 0.83	L_{hHz}
24.56 ± 0.63	1.23 ± 0.18	9.80 ± 0.67	L_h
13.32 ± 0.41	2.15 ± 0.56	5.39 ± 0.84	L_{LF}
5.64 ± 0.48	0.09 ± 0.04	13.77 ± 0.47	L_b
Power spectrum B			
ν_{max} (Hz)	Q	rms (%)	comp.
527.99 ± 7.32	3.25 ± 0.41	9.46 ± 0.45	L_u
154.20 ± 8.80	0.72 ± 0.14	9.81 ± 0.53	L_{hHz}
29.48 ± 0.74	1.16 ± 0.14	9.15 ± 0.52	L_h
16.60 ± 0.35	2.50 ± 0.47	4.91 ± 0.60	L_{LF}
7.49 ± 0.48	0.10 ± 0.04	12.94 ± 0.35	L_b
Power spectrum C			
ν_{max} (Hz)	Q	rms (%)	comp.
537.98 ± 6.68	2.98 ± 0.34	9.61 ± 0.41	L_u
177.08 ± 7.90	0.82 ± 0.14	9.61 ± 0.47	L_{hHz}
30.06 ± 0.64	1.05 ± 0.13	8.83 ± 0.49	L_h
16.30 ± 0.28	3.66 ± 1.00	3.39 ± 0.52	L_{LF}
9.14 ± 0.66	0.04 ± 0.03	14.05 ± 0.40	L_b
Power spectrum D			
ν_{max} (Hz)	Q	rms (%)	comp.
578.98 ± 7.30	3.71 ± 0.47	10.14 ± 0.48	L_u
184.59 ± 12.70	0.86 ± 0.23	8.93 ± 0.75	L_{hHz}
27.86 ± 1.65	0.41 ± 0.11	12.73 ± 1.23	L_h
8.18 ± 1.19	0.15 ± 0.05	11.06 ± 1.18	L_b
Power spectrum E			
ν_{max} (Hz)	Q	rms (%)	comp.
675.01 ± 4.06	4.58 ± 0.41	8.54 ± 0.27	L_u
407.94 ± 30.54	$3.85^{+5.13}_{-1.82}$	2.81 ± 0.85	L_ℓ
170.37 ± 14.67	0.98 ± 0.42	6.65 ± 1.44	L_{hHz}
61.69 ± 3.69	0.77 ± 0.26	8.33 ± 1.27	L_h
29.61 ± 0.46	2.80 ± 0.53	4.00 ± 0.48	L_{LF}
14.41 ± 0.25	1.06 ± 0.25	6.89 ± 1.33	L_b
9.94 ± 3.77	0.00 ± 0.00	7.73 ± 1.77	L_{b2}^a

Power laws Parameters			
Power spectrum	PL index	rms (%)	Integration Interval (Hz)
A	1.9 ± 0.5	1.19 ± 0.15	0.01 – 0.08
B	1.6 ± 0.4	1.2 ± 0.1	0.01 – 0.06
E	2.22 ± 0.24	1.02 ± 0.53	0.01 – 0.08

Table 5.2: Characteristic frequencies ν_{max}, Q values ($\equiv \nu_0/FWHM$ – see Section 5.2), Integrated fractional rms (of the full PCA energy band) and identification (comp.) of the Lorentzians fitted for 4U 1820–30. The quoted errors in ν_{max}, Q and rms use $\Delta\chi^2 = 1.0$. ^{a}: Lorentzian with $\sim 2.7\sigma$ significance.